

Slow dynamics under gravity: a nonlinear diffusion model

Jeferson J. Arenzon* and Yan Levin†

*Instituto de Física, Universidade Federal do Rio Grande do Sul
CP 15051, 91501-970 Porto Alegre RS, Brazil*

Mauro Sellitto‡

*Abdus Salam International Centre for Theoretical Physics
Strada Costiera, 11, 34100 Trieste, Italy*

(Dated: October 31, 2018)

We present an analytical and numerical study of a nonlinear diffusion model which describes density relaxation of loosely packed particles under gravity and weak random (thermal) vibration, and compare the results with Monte Carlo simulations of a lattice gas under gravity. The dynamical equation can be thought of as a local density functional theory for a class of lattice gases used to model slow relaxation of glassy and granular materials. The theory predicts a jamming transition line between a low density fluid phase and a high density glassy regime, characterized by diverging relaxation time and logarithmic or power-law compaction according to the specific form of the diffusion coefficient. In particular, we show that the model exhibits history dependent properties, such as quasi reversible-irreversible cycle and memory effects – as observed in recent experiments, and dynamical heterogeneities.

I. INTRODUCTION

The dynamics of granular matter has received considerable attention in the past few years as it poses interesting problems from a theoretical point of view, besides its relevance to industrial applications [1, 2, 3, 4]. At high density, excluded-volume interactions play a crucial role in the formation of disordered, amorphous granular packings. In fact, the analogy between slowly compacting granular materials and other disordered systems like glasses has been early recognized [5, 6], and has motivated several experiments in which slow compaction and history dependence have been investigated in great detail [7, 8, 9, 10, 11].

Granular and glassy systems share the important feature of having an exponentially large number (in the system size) of different mechanically stable packings. Microscopically, this property can be thought of as generated by geometric frustration or kinetic constraints on the possible moves or positions of particles. This in turn leads, at high packing density, to a vanishing particle mobility which is the distinctive macroscopic manifestation of slow relaxation and jamming transition (dynamical arrest).

In general, two ingredients are responsible for the unusual behavior of a granular material. First, collisions between the particles are inelastic, and energy has to be constantly pumped into the system. Second, at high packing density, the excluded volume, and the associated cage effect, is very similar to the one observed in structural glasses [12]. A number of schematic lattice-

gas models [13, 14, 15, 16, 17, 18, 19] has shown indeed that the main features of irreversible compaction do not depend, to a certain extent, on the dissipation mechanism (which is often assumed to be, for simplicity, of thermal nature), but can be understood solely in terms of steric hindrance. In this paper, we shall be concerned precisely with this quasi-static flow regime, which in the case of dense systems is the relevant one. Even with this simplifying assumption the detailed correspondence with mean-field, mode-coupling approaches of glassy dynamics remains however problematic because the presence of gravity leads to a non-trivial dependence on the spatial variable for the basic observables. Other complications may further arise from the presence of boundary conditions. At the present stage, coarse-grained approaches based on real-space diffusion equations can therefore be very useful in the theoretical interpretation of experimental results and to disentangle the glassy features which are inherent to the compaction dynamics from the ones which depend on the specific energy injection/dissipation mechanism.

Some typical questions in slow granular dynamics that one is concerned with are the:

- origin of the logarithmic compaction law;
- scaling behavior of the aging dynamics;
- reversible-irreversible cycle;
- memory phenomena;
- and dynamical heterogeneities.

We have recently addressed some of these issues by studying the dynamics of a kinetic free-volume model for granular media [15], and proposing an analytical approach based on a dynamical local density functional theory [20]. We have precisely characterized the way compaction and aging depend on the particle mobility of a

*Electronic address: arenzon@if.ufrgs.br

†Electronic address: levin@if.ufrgs.br

‡Electronic address: sellitto@ictp.trieste.it

homogeneous system. Specifically, there are two relaxation regimes, fast and slow, separated by a dynamic jamming transition. The compaction law in the slow dynamic regime depends upon the particle mobility: we find that logarithmic compaction and simple aging are intimately related to the Vogel-Fulcher law, while power-law compaction and superaging behavior occur in the presence of a power-law vanishing mobility. The objective of this paper is to extend our previous work [15, 20], and in particular to address other history dependent phenomena, such as reversible-irreversible cycles [8, 9, 10], memory phenomena [21, 22, 23, 24] and dynamical heterogeneities [25, 26], which have recently attracted some attention.

In the next section we shall introduce the nonlinear diffusion model and the related lattice-gas which is thought to be its microscopic realization. The stationary density profiles, along with the jamming transition will be presented in section III. In section IV the possible scenarios for the time evolution of packing density are described. Reversible-irreversible cycles and memory phenomena will be discussed in section V, while the scaling behavior of the aging dynamics is addressed in section VI. Section VII discusses the dynamical heterogeneities in presence of gravity and, finally, in section VIII the conclusions will be presented.

II. MODELS

A. Nonlinear diffusion equation

We assume that the dynamical evolution of the local particle density $\rho(z, t)$ is governed by the continuity equation,

$$\frac{\partial \rho(z, t)}{\partial t} + \frac{\partial J(z, t)}{\partial z} = 0 ,$$

with the particle current $J(z, t)$ given by the Fick's law,

$$J(z, t) = -\Gamma(\rho) \frac{\partial \mu(z, t)}{\partial z} ,$$

where $\Gamma(\rho)$ is the Onsager mobility and $\mu(z, t) = \frac{\delta F}{\delta \rho}$ is the local chemical potential. The only interaction between the grains we consider is the hard core repulsion, for which the exact lattice Helmholtz free energy functional is [27]

$$\beta F[\rho(z, t)] = \int_0^H dz [\gamma z \rho - S(\rho)] , \quad (1)$$

where the entropy $S(\rho)$ is given by

$$S(\rho) = -\rho \ln \rho - (1 - \rho) \ln(1 - \rho) . \quad (2)$$

For highly packed hard-sphere systems, theoretical and experimental studies suggest that the diffusion coefficient

vanishes as a power-law [28, 29, 30]. Hence we will assume that the mobility $\Gamma(\rho)$ vanishes as

$$\Gamma(\rho) = \Gamma_0 \rho \left(1 - \frac{\rho}{\rho_c} \right)^\phi ,$$

and remains zero for $\rho > \rho_c$. Below we will also discuss another possible functional form for the mobility which is commonly encountered in systems of particles with anisotropic shape (e.g. rods). Note that the above functional form of mobility has an implicit dependence on the height, because the density profile is typically inhomogeneous ($\rho = \rho(z)$) due to the driving force and boundary conditions. The use of a local density approximation for the mobility will be justified by the comparison of theoretical predictions with Monte Carlo simulations of a lattice gas model which exhibits a vanishing diffusion coefficient at a threshold density ρ_c [31]. Substituting $\Gamma(\rho)$ into the continuity equation we are led to

$$\frac{\partial \rho}{\partial t} = \frac{\partial}{\partial z} \left\{ \left(1 - \frac{\rho}{\rho_c} \right)^\phi \left[\frac{1}{1 - \rho} \frac{\partial \rho}{\partial z} + \gamma \rho \right] \right\} , \quad (3)$$

where the time is now measured in units of $1/\Gamma_0 k_B T$. This equation has to be completed by specifying the boundary conditions. We will discuss two simple cases corresponding to open and closed systems. In both situations one boundary condition requires the vanishing of the current at the bottom layer $z = 0$, $J(0, t) = 0$ for any time t . If the top layer $z = H$ is in contact with a particle reservoir at density ρ_R (open system), the other boundary condition reads $\rho(H, t) = \rho_R$ for all t ; while for a closed system in which the total number of particles is kept constant, the second boundary condition leads to a vanishing current also at $z = H$, $J(H, t) = 0$. Although no closed analytical solutions of Eq. (3) is found, it is possible to characterize its asymptotic long time regime by an explicit calculation of density relaxation and two-time mean-square displacement.

B. Microscopic lattice gas

The simplest microscopic realization of the nonlinear diffusion equation one can imagine is provided by a lattice gas having a vanishing diffusion coefficient above a certain threshold density (see [32] and references therein). A paradigmatic example is the kinetically constrained lattice gas model devised by Kob and Andersen [31]. The model was originally introduced with the purpose to test the predictions of the mode-coupling theory for supercooled liquids [28]. The system consists of N particles on a lattice with at most one particle per site and no other static interactions between the particles, that is the Hamiltonian is $\mathcal{H} = 0$. The microscopic dynamic is as follows: at each time step a particle and one of its neighboring sites are chosen at random; the particle can move to the new site if this site is empty and if the particle has

less than ν nearest neighbors occupied *before* and *after* the move. This kinetic rule is time-reversible and the detailed balance is satisfied. At high densities, the dynamics slows down because the reduced free-volume makes it harder for a particle to satisfy the dynamic constraints. There exists a critical density ρ_c above which the particles are so interlocked that no macroscopic structural rearrangement is possible and the mobility falls to zero as a power law, $D(\rho) \sim (\rho_c - \rho)^\phi$. For the simple cubic lattice [31], $\rho_c \simeq 0.88$, while for the body centered cubic (BCC) lattice one gets $\rho_c \simeq 0.84$, see Fig 1. The critical density ρ_c is therefore non universal, depending both on the lattice structure and the particular choice of the dynamical constraint parameter ν . In both cases, however, the value of the exponent is consistent with $\phi \simeq 3.1$. The universality of the exponent ϕ was recently suggested by Imparato and Peliti, who studied the diffusion on a face centered cubic lattice for several choices of ν [33].

Since much of dynamical properties of both structural glasses and dense granular materials are dictated by steric constraints, we have generalized [15] the Kob-Andersen model in a gravitational field. The Hamiltonian now is

$$\beta\mathcal{H} = \gamma \sum_i z_i n_i \quad (4)$$

where $n_i = 0, 1$ is the occupation variable of the i -th site whose height is z_i , $\gamma = mg/k_B T$ is the inverse gravitational length and g is the constant gravitational field acting in the $-z$ direction. Since we are interested in the slow compaction regime, the energy dissipation due to inelastic collisions is ignored. The thermal energy of the grains is negligible and T is neither the physical temperature nor the “granular temperature” usually associated with the average kinetic energy, but rather a function of the externally imposed vibration intensity. In other words, we assume that the random diffusive motion of “grains” produced by the mechanical vibrations of the box can be modeled as a thermal bath of temperature T [50]. The particles satisfying the kinetic constraints can move according to the Metropolis rule with probability $\min[1, x^{-\Delta h}]$, where $\Delta h = \pm 1$ is the vertical displacement for the attempted elementary move and $x = \exp(-\gamma)$ represents the “vibration amplitude”. Particles are confined in a box closed at the bottom and with periodic boundary condition in the horizontal direction. At the top, the box can be either closed or in contact with a particle reservoir. We set the constraint threshold at $\nu = 5$. The Markov process generated by the kinetic rules is irreducible on the full configuration space [15], the static properties of the model are those of a lattice-gas of non-interacting particles in a gravitational field, and these can be easily computed. For example, the mean occupation of each level is:

$$\rho(z) = \frac{1}{1 + e^{\gamma(z+\eta)}}, \quad (5)$$

where the Lagrange multiplier η is determined by the

global density or the chemical potential, according to the statistical ensemble.

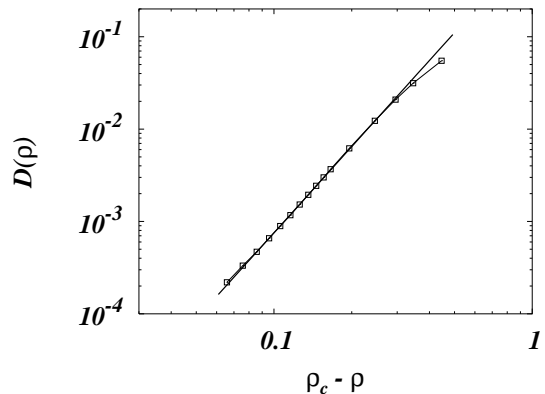


FIG. 1: The diffusion coefficient of a BCC lattice ($L = 32$) as a function of the density. The full line is a power-law fit with $\rho_c \simeq 0.84$ and $\phi = 3.1$.

III. JAMMING TRANSITION AND DENSITY PROFILES

A. Open system

The stationary state of Eq. (3) is obtained when $\partial\rho/\partial t = 0$, which implies that $J(z, \infty) = 0$ for all z . Imposing the stationarity condition, depending on the value of γ , two very distinct types of stationary profiles are found. For high values of γ the system is in equilibrium and the profile is given by Eq. 5. As the vibration is lowered, a homogeneous region of constant density $\rho(z, \infty) \equiv \rho_c$ develops below the height z_0 . The stationary solution of Eq. 3 becomes,

$$\rho_\infty(z) = \begin{cases} \rho_c, & z \leq z_0 \\ \frac{1}{1 + \exp(\gamma z + \eta)}, & z \geq z_0 \end{cases} \quad (6)$$

The values of z_0 and η are obtained from the boundary conditions. If the top of the box is connected to a particle reservoir then $\rho_\infty(H) = \rho_R$. This and the continuity of the density profile at $z = z_0$ lead to,

$$z_0 = H + \frac{1}{\gamma} \ln \frac{\rho_R(1 - \rho_c)}{\rho_c(1 - \rho_R)} \quad (7)$$

$$\eta = \ln \frac{1 - \rho_R}{\rho_R} - \gamma H. \quad (8)$$

The jamming transition corresponds to the locus in the parameter space (γ, ρ_R) , at which the $z = 0$ layer attains the critical density so that $\rho(0, \infty) = \rho_c$. This happens when

$$\gamma_c(\rho_R) = \frac{1}{H} \ln \frac{\rho_c(1 - \rho_R)}{\rho_R(1 - \rho_c)}. \quad (9)$$

When $\gamma > \gamma_c(\rho_R)$ the density at the bottom of the box is close to the critical and dynamics becomes sluggish. On the other hand, above the critical temperature, $\gamma \leq \gamma_c(\rho_R)$, all the layers have densities smaller than ρ_c and the system easily attains equilibrium. The critical line Eq. 9 is plotted, as a function of ρ_R , in Fig. 2. Notice that for the undriven case ($\gamma = 0$) the transition only occurs if $\rho_R = \rho_c$. It is important to stress that for $\gamma > \gamma_c(\rho_R)$ the stationary profiles Eq. 6 are not equivalent to the equilibrium ones since they do not minimize the Helmholtz free energy functional Eq. 1. This is so because the system is not able to achieve, dynamically, densities higher than ρ_c . In the zero gravity case $\gamma = 0$, the stationary profile is flat, $\rho_\infty(z) = \rho_R$.

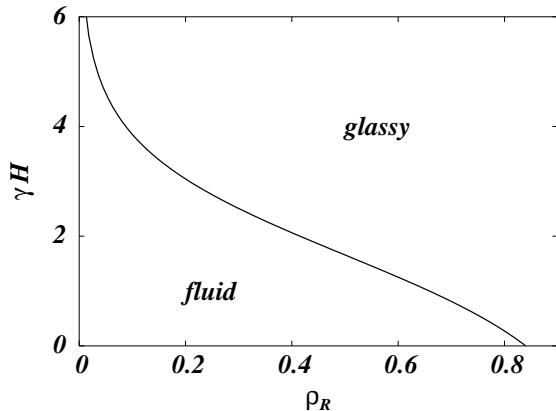


FIG. 2: Jamming transition line γ_c (multiplied by H) as a function of ρ_R , from Eq. 9. This line separates regions of slow (glassy) and fast (fluid) relaxation.

In Fig. 3 we compare the stationary profiles with the ones found in Monte Carlo simulation of the gravity-driven KA model on the BCC lattice [15, 20] at large times. A very good agreement is obtained with no adjustable parameters. As discussed in the next section, the simulations were carried on connecting the topmost layer of the system to a reservoir of particles.

B. Closed system

For a closed system of volume V (the height H times the basis area) and a fixed number of particles $N = \bar{\rho}V$ one proceeds in a way analogous to the previous section. We find that z_0 and η satisfy the coupled equations

$$z_0 = \frac{1}{\gamma} \ln \frac{1 - \rho_c}{\rho_c} - \frac{\eta}{\gamma} \quad (10)$$

$$\eta = \ln \frac{e^{-\gamma[\bar{\rho}H + z_0(1 - \rho_c)]} - e^{-\gamma H}}{1 - e^{\gamma(\rho_c z_0 - H\bar{\rho})}}. \quad (11)$$

while the locus of the jamming transitions satisfies the implicit equation

$$\gamma_c = -\frac{1}{\bar{\rho}H} \ln(1 - \rho_c + \rho_c e^{-\gamma_c H}) \quad (12)$$

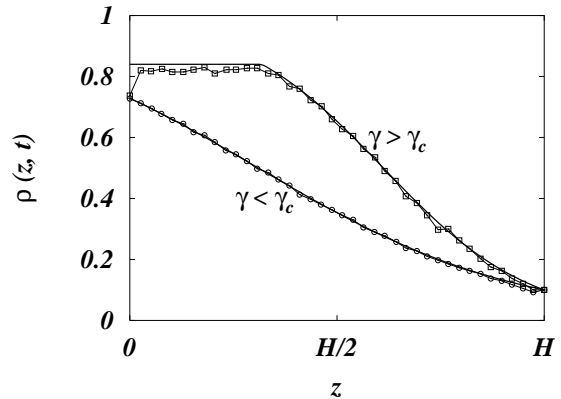


FIG. 3: Stationary profiles above and below the critical line for an open system in contact with a particle reservoir at density $\rho_R = 0.1$. The symbols are the densities obtained from the simulation on a BCC lattice and the solid lines are the theoretical results. For $\gamma = 0.072 > \gamma_c$, squares, the longest time shown is 10^6 MCS while for $\gamma = 0.041 < \gamma_c$, circles, the time is 10^5 MCS. Notice that the simulation profile for $\gamma > \gamma_c$ is not yet stationary.

This line is depicted in fig. 4 as a function of the average density $\bar{\rho}$. An example of a stationary profile for a fixed number of particles is shown in fig. 5. Simulations on bidimensional hard spheres also present a profile compatible with an almost flat part plus an interface [34].

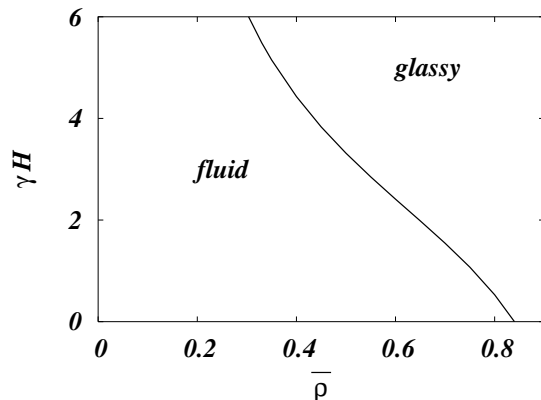


FIG. 4: Jamming transition line, γ_c (multiplied by H), as a function of the average density $\bar{\rho}$. The divergence near the origin scales as $\bar{\rho}^{-1}$, different from the logarithmic divergence found for the system in contact with a reservoir, Eq. 9. Notice that in this case the density parameter is the average total density, $\bar{\rho}$, while in the open case it is the reservoir density ρ_R .

We now turn to the behavior of the density profile found in the Monte Carlo simulation. We first let the system evolve at $x = 0$ until a mechanically stable configuration in which no particle can move down, is achieved. This state is metastable because at $x = 0$, there is a single ground state with equilibrium bulk packing density $\rho = 1$. Experimentally, it has been verified that the ini-

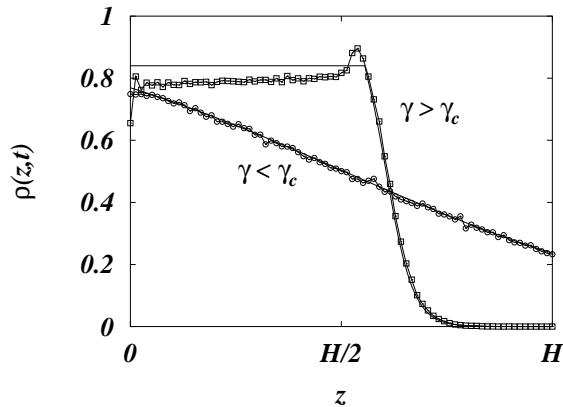


FIG. 5: Examples of density profiles above and below the critical line for a system closed after its density achieved $\bar{\rho} = 0.5$. The tapping amplitude in the glassy phase is $\gamma = 0.4$, while in the fluid phase it is $\gamma = 0.03$; system height $H = 80$. Notice that for $\gamma > \gamma_c$ the profile at finite times (10^6 MCS in this case) is neither stationary nor flat.

tial density depends on the preparation procedure [35], in particular, on the box filling rate, that is, the number of particles which fall per unit of time. If particles are poured one at a time, that is, they are individually handled, then the falling trajectories are independent. By doing so in the gravity driven KA model, the kinetic constraints would always be satisfied since the sites above the falling particle would be empty, and the system would achieve a fully compacted state. By pouring more than one particle at a time, their trajectories may interfere, preventing the system from achieving the highest possible density. This collective handling of particles may be implemented in several ways. For example, in ref. [15], in order to avoid this highly compacted initial state, all the particles were poured together, by placing them in the upper half of the box and letting them fall randomly under the action of the gravitational field, until a state where no particles can fall further is achieved. In this case the initial average packing density is $\rho_{\text{flp}} \simeq 0.707$, roughly corresponding to a random loose packed state. Once the system is prepared, the vibration at a fixed amplitude x is turned on. Another possibility, pointed out in the previous section is to use a reservoir that may be left open forever or be closed after a predetermined number of particles has entered the box. This is also a collective way of handling the particles, with the advantage that the initial flux of particles can be tuned, being intermediate between all particles falling at once and one at a time. Indeed, as the system is less constrained than when all the particles are falling at once, it is able to achieve a larger bulk density and the profile is closer to the stationary one (see figs. 3 and 5). Moreover, for the same reason, the structured region at the bottom, discussed in [15], is either absent or significantly less pronounced.

Near the top of the granular pile, a dense interfacial layer forms as a result of an increased mobility due to the low density of particles in the top most layers. This dense layer becomes more compact with time hindering the underneath particles motion. However, due to the (horizontal) roughness of the interface the effect appears less pronounced than in the bottom region. On the other hand, if the reservoir is kept open for all times, there is no such sudden decrease in density, and even particles at the interface are still quite constrained and no dense layer is observed in the profile shown in the previous section (fig. 3).

IV. COMPACTION DYNAMICS

A. Low density phase

Above the jamming transition, $\gamma < \gamma_c(\rho_R)$, the approach to equilibrium is exponentially fast, $\rho(z,t) \simeq \rho_\infty(z) + g(z)e^{-t/\tau}$, as can be checked by numerically solving Eq. 3.

When the system is in permanent contact with a reservoir, the characteristic time satisfies an *exact* scaling equation [20]

$$\tau^{-1} = \frac{\pi^2}{4H^2} \mathcal{F}(\gamma H; \rho_R), \quad (13)$$

where $\mathcal{F}(y; \rho_R)$ is a scaling function. In the special case of zero gravity [36], $\gamma = 0$, particles diffuse freely from the reservoir until a uniform density, $\rho_\infty(z) = \rho_R$, is established. The characteristic time of approach to equilibrium can be calculated explicitly [20] by linearizing Eq. 3. We find that the relaxation time for $\gamma = 0$ is

$$\tau^{-1} = \frac{\pi^2}{4H^2(1 - \rho_R)} \left(1 - \frac{\rho_R}{\rho_c}\right)^\phi, \quad (14)$$

or equivalently $\mathcal{F}(0; \rho_R) = (1 - \rho_R/\rho_c)^\phi / (1 - \rho_R)$. Eq. 14 is in perfect agreement with the numerical integration of Eq. 3 [20]. As expected, the relaxation time diverges as $\rho_R \rightarrow \rho_c$. The exponent characterizing this divergence is ϕ .

In the presence of a gravitational field we find, by numerical integration of Eq. 3, that as $\gamma \rightarrow \gamma_c(\rho_R)$, the density of the first layer approaches ρ_c , $\rho_\infty(0) \rightarrow \rho_c$, and $\mathcal{F} \sim (\gamma_c - \gamma)^{\phi-2}$. Thus, the relaxation time diverges with exponent $\phi - 2$, see fig. 6, implying that the dynamics is faster than in the zero gravity case. Comparing with Eq. 14, we see that the jamming transitions in the homogeneous and inhomogeneous systems, belong to distinct dynamic universality classes.

B. High density phase

Below the jamming transition, $\gamma > \gamma_c(\rho_R)$, the density of the bottom layers, $z < z_0(\rho_R)$, is close to the critical,

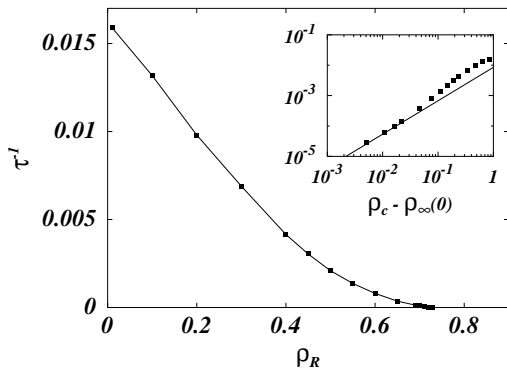


FIG. 6: Inverse relaxation time, τ^{-1} , for $\gamma = 0.1$ and $H = 10$ with $\rho_c = 0.88$ and $\phi = 3.1$, corresponding to the Kob-Andersen model on a simple cubic lattice. The points are the result of numerical integration of Eq. 3. Inset shows the same data on the log scale. The characteristic time diverges with exponent $\phi - 2$ as the jamming transition is approached.

$\rho(z, t) \simeq \rho_c$, and the dynamics slows down. To the lowest order in $\Delta(z, t) \equiv 1 - \rho(z, t)/\rho_c$, Eq. 3 simplifies to,

$$\frac{\partial \Delta(z, t)}{\partial t} = -\gamma \frac{\partial \Delta^\phi}{\partial z}. \quad (15)$$

To solve this non-linear equation we propose a scaling ansatz $\Delta(z, t) = \Delta(z/t^\alpha)$. Substituting into Eq. 15 we see that this form is a solution if $\Delta(z/t^\alpha)$ is a power law with $\alpha = 1$:

$$\Delta(z, t) = \left[\frac{z}{\gamma \phi t} \right]^{\frac{1}{\phi-1}}. \quad (16)$$

Notice, that in the absence of gravity, $\gamma = 0$, density relaxation is slower and characterized by a different dynamical exponent, $\Delta(z, t) \sim t^{-1/\phi}$ [36].

Although in experiments one is usually interested in the bulk properties, Eq. 3 can also shed some light on how the upper layers $z > z_0$ compact. Using the asymptotic solution, Eq. 16, in the definition of $J(z, t)$ we find that for large times the particle current passing from the upper layers into the bulk through $z = z_0$ is

$$J(z_0, t) = \gamma \rho \left(\frac{z_0}{\gamma \phi t} \right)^{\frac{\phi}{\phi-1}}. \quad (17)$$

Since the density of the upper layers is smaller than critical and since we are only interested in the scaling behavior, it is sufficient to study the linearized version of Eq. 3

$$\frac{\partial \rho}{\partial t} = \frac{\partial^2 \rho}{\partial z^2} + \gamma \frac{\partial \rho}{\partial z}, \quad (18)$$

with boundary condition: $\rho(H, t) = \rho_R$, and $J(0, t) = J(z_0, t)$. The temporal Laplace transform of this linear equation can be easily solved yielding for the density relaxation of upper layers the following expression:

$$\rho(z, \infty) - \rho(z, t) \simeq \frac{J(z_0, t)}{\gamma} \left[e^{\gamma(H-z)} - 1 \right] \sim t^{-\frac{\phi}{\phi-1}} \quad (19)$$

Remarkably, the time relaxation above and below z_0 are both slow and follow a power law with different exponent. As expected, the dynamics in the upper layers is faster than in the lower ones, and its contribution to the relaxation function at long times becomes negligible since ϕ is usually larger than one.

The asymptotic solution, Eq. 16, is in partial agreement with the lattice-gas Monte Carlo simulation data, Fig. 7. The same numerical data were previously fitted with a four parameter logarithm law

$$\rho(t) = \rho_\infty - \frac{\Delta \rho_\infty}{1 + B \ln(1 + t/\tau)}, \quad (20)$$

where ρ_∞ is the asymptotic packing density and B , $\Delta \rho_\infty$ and τ are adjustable parameters which also depend on x . The above function, first used in Ref. [7], gives a reasonable fit in the whole time window accessible to experiments; however, one can check that the long time behavior is also compatible with a power law relaxation. Interestingly enough, something similar happens here, confirming that a limited time-window may not allow to distinguish among several regimes of slow relaxation [37]. One can also notice, from fig. 7 that for high values of x , all curves are compatible with the same exponent, while for small values, the exponents seems to be different. This may be however another artifact of the very slow relaxation for small x , which prevents the system from attaining the asymptotic regime.

Further, we find that independently of the specific functional form of the fit, logarithmic or power law, the asymptotic packing density $\rho_{25\%}^\infty$ is quite the same for the simulation data, Fig. 8. It turns out to be a non monotonic function of vibration x and displays an optimal value for the asymptotic compaction, as can be seen in Fig. 8. This maximum is achieved for rather high vibration because an initial decompaction increases the free volume available to particles making it easier to satisfy the kinetic constraints and their local arrangements. It is clear that the specific location of the maximum depends on the portion chosen to measure the packing density ($H/4$ in this case) however it does not affect the form of the plot.

Finally, in order to stress the counterintuitive nature of compaction dynamics it is worth to point out its relationship with the so-called negative resistance phenomena. These are usually observed in a non-equilibrium stationary state, where an increasing driving force leads to a decreasing system response (usually a particle current). During irreversible compaction, which is non-stationary, something similar happens: indeed, when vibration (the driving force) increases the *a priori* probability that a particle moves upward is larger; it actually turns out that the system compacts, i.e. the average direction of particle flow (the response) is preferentially downward and non-monotonic. This is illustrated in Fig. 9 where we plot the local current $J(z, t)$ at different times t , as a function of the vibration strength x . One observes that at any given time, there is an optimum value of x at which the cur-

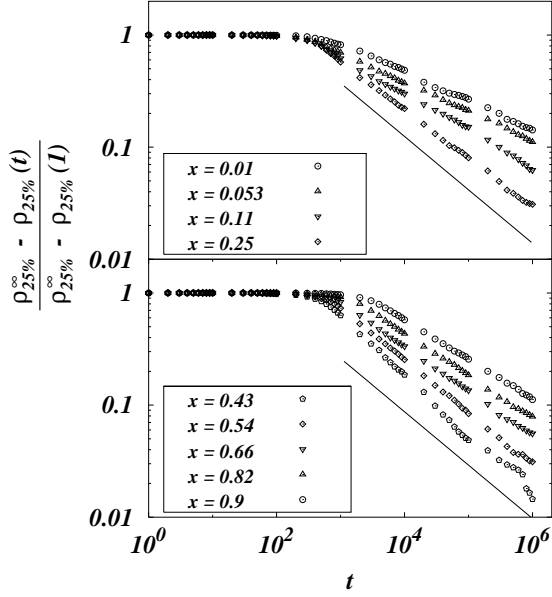


FIG. 7: Power law fit (normalized to unity), for large times, of compaction data. The fit parameters are all dependent on x , although a unique exponent for the large values of x is also consistent. The full straight line $t^{-1/(\phi-1)}$ represent the long-time prediction of the nonlinear diffusion equation.

rent get its maximum. At increasing time the maximum moves towards higher values of x . Qualitatively similar results are obtained for different z .

C. Logarithmic compaction and Vogel-Fulcher law

Up to now our discussion has been motivated by dynamics which are characterized by a power-law vanishing mobility. However, there are various systems for which the mobility vanishes according to the Vogel-Fulcher law [11],

$$\Gamma(\rho) = \Gamma_0 \rho \exp\left(\frac{a\rho_c}{\rho - \rho_c}\right). \quad (21)$$

Boutreux and de Gennes [38] have argued that logarithmic compaction is intimately related to this Vogel-Fulcher law which in turns derive from a Poisson distribution of voids in the systems. A similar conclusion can also be drawn from our approach. In this case the time evolution of the local particle density is governed by the equation

$$\frac{\partial \rho}{\partial t} = \frac{\partial}{\partial z} \left\{ \exp\left(\frac{a\rho_c}{\rho - \rho_c}\right) \left[\frac{1}{1 - \rho} \frac{\partial \rho}{\partial z} + \gamma \rho \right] \right\}. \quad (22)$$

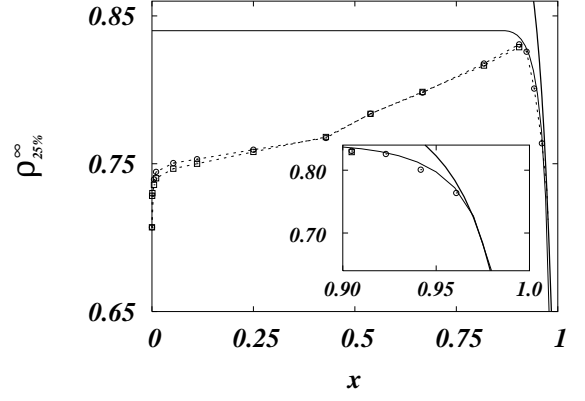


FIG. 8: Square and circle symbols are the asymptotic packing densities obtained within the Monte Carlo simulation with fixed number of particles. The two refer to the extrapolations using a power law fit and the logarithmic form, Eq. 20. The equilibrium density is the thick solid line while the thin line is the bulk density evaluated from the asymptotic limit of Eq. 6, 10 and 11. The dynamical jamming transition is located where all curves meet, near $x_c \simeq 0.979$. Notice that, from the theory, up to the region near the maximum we have $z_0 > H/4$ and the packing density is ρ_c , while above it the point z_0 penetrates in the defined bulk region and the density deviates from ρ_c . Inset: region near the transition. Notice that the simulation data agree well with the result from the diffusion equation, while below x_c both start to deviate from the equilibrium curve.

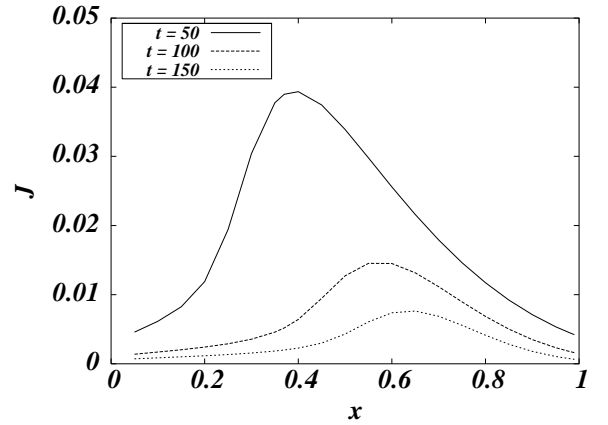


FIG. 9: Local current $J(z, t)$ for several times t and $z = H/2$, as a function of the vibration strength x .

Again, proceeding as in the previous section, to the lowest order in $\Delta(z, t) \equiv 1 - \rho(z, t)/\rho_c$, one finds that for the bottom layers ($z < z_0$)

$$\frac{\partial \Delta(z, t)}{\partial t} = -\gamma \frac{\partial}{\partial z} \exp\left[-\frac{a}{\Delta(z, t)}\right]. \quad (23)$$

As before we attempt a scaling ansatz. For very large times we find

$$\Delta(z, t) = \frac{a}{\ln(t/z)}, \quad (24)$$

which is in agreement with the full numerical solution of Eq. 3. This relaxation is similar to the logarithmic compaction law, Eq. 20 used to fit experimental data by Chicago group [7].

For layers above z_0 , the time evolution is still slow but follows a power law. Proceeding in the same way used to obtain Eq. 19 we find

$$\rho(z, \infty) - \rho(z, t) \sim t^{-1}. \quad (25)$$

Although the bulk dynamics is logarithmically slow, the compaction of upper layers is governed by a power law with exponent -1 .

V. HISTORY DEPENDENCE

It is well known that dynamical effects in slow relaxing systems depend sensitively on the history of the sample after a quench in the high density (or low temperature) phase. These phenomena have been extensively studied by means of several experimental protocols.

In the previous section we focused on the simplest situation in which the sample is prepared in a random loose packed state and then the vibration is turned on and kept fixed to a given value of amplitude during the measurement.

In order to test the system response, here we consider the effects of cyclic changes in the vibration amplitude, either continuously or suddenly, to a different value which corresponds to a state with a lower or higher asymptotic packing density.

A. ‘Reversible’-irreversible cycles

Experiments on glass beads [8, 9] have shown that under a cyclic variation of the vibration a system prepared in a random loose packed state first presents a branch during which the density increases as a function of the vibration (until high vibrations are attained and decompaction starts). This branch is irreversible, meaning that when the vibration is decreased at the same rate, the system does not trace back the earlier evolution, but rather its density keeps growing as the vibration decreases. Experimentally this second branch appears to be reversible, that is, the system seems to reach a stationary state in which any further cyclic variation of the vibration keeps the system always on the second branch. Along this branch the packing density is a decreasing function of the vibration amplitude (contrary to what happens in the irreversible compaction regime).

Applying the same protocol to both the diffusion equation and the lattice-gas we find that the reversible branch

only appears for extremely slow driving rates. Similar results have been observed experimentally during the compaction of anisotropic granular materials like rods [10] and shearing induced compaction [22]. The system presents a succession of irreversible branches which get closer and closer as the number of cycles increases (see Figs. 10 and the corresponding inset). The slower the vibration change rate is, the smaller is the separation between the branches. In this way, for real systems the distance between the irreversible branches can become of the order of the measurement error, appearing as if there was just one reversible branch. It must be noticed that after cycling for a certain number of times, the density hardly changes from the lowest to the highest values of x , presenting a rather flat behavior. This can be explained using the asymptotic packing density, fig 8: unless the vibration is too high, the asymptotic bulk profile is flat. Even if the system enters in the high- x region, the flatness of the density will depend on the vibration change rate. Finally, we mention that for some choices of the parameters small hysteresis [39] loops also appear in the region of high vibration; the area of the loops is a function of the vibration rate. We also expect that by using the Vogel-Fulcher mobility the cycles present a very similar behavior. Moreover, for high vibrations, dissipation effects may play a role. It would be interesting to experimentally study particles with different friction properties to check to what extent the cycle properties depend on these. In fig. 11 we illustrate the effect of changing the turning point, that is, the maximum attained value of x before starting to decrease it. We notice that the density follows almost parallel paths, only that the maximum attained density is bigger the higher is the turning point.

B. ‘Memory’ effects

Another possible experiment devised to explore history dependence consists of measuring the short-time response of an aged system to an abrupt perturbation in x [21, 22]. After evolving the system for a certain t_w at a fixed x , the vibration amplitude is shifted by Δx until the time $t_w + \Delta t$ and then returned to x . As an example, in Fig. 12, we show the curves for perturbations applied to systems with different age, $t_w = 10^3$ and $t_w = 10^4$. In both cases, $\Delta x < 0$, and the compaction rate increases while one would expect, from the long term behavior of the system, a slower relaxation for a smaller value of x . For the older system, $t_w = 10^4$, the first regime is hardly visible because the system is stiffer. These results, are consistent with earlier experimental [21] and theoretical [23, 24, 37] works. For $\Delta x > 0$ (not shown), although one would expect a faster compaction, for short times soon after the perturbation the system decompacts. The same behavior is also found for the diffusion equation when the system is in contact with the particle reservoir. For large times after turning the perturbation off, the system resumes its normal behavior. Thus, because

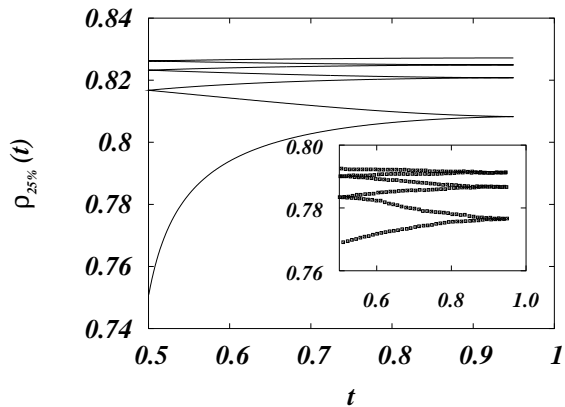


FIG. 10: Bulk density as a function of time for a cycling variation of the driving rate within the nonlinear diffusion equation (Eq. 3). Here the waiting time is 500 steps and the reservoir is again at $\rho_R = 0.1$. Each branch evolves from 5×10^3 steps from the minimum x value of 0.5 to the maximum one of 0.95. Inset: the same experiment with the gravity driven KA lattice-gas model. The parameters are the same as before, only that the waiting time is 5000 MCS and each branch has a total duration of 2×10^4 MCS. In both cases, the distance between the branches decreases as the number of cycles increases.

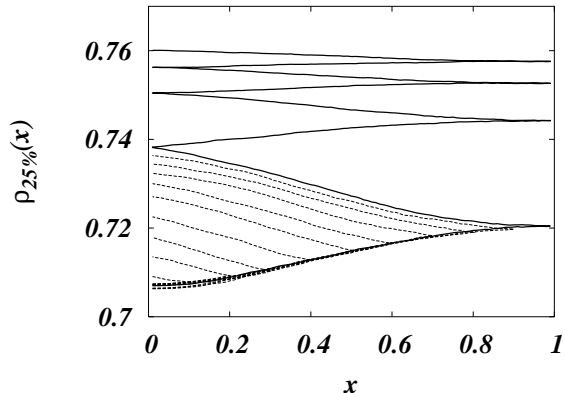


FIG. 11: The same as the inset of fig. 10 only that x is reversed at different maximum values. Notice that in this case, different densities are attained.

of the transient nature of the response, it appears as a short-term memory. Moreover, after the initial anomalous behavior, the perturbed and non perturbed curve crosses and the system start to evolve with the rate expected from long term behavior.

Besides short-term memory effects, long-term memory is also present. To see this, we repeat the above experiments with the difference that the perturbation is applied at a much larger t_w (10^5 in this case). Moreover, the perturbation is kept on also for a longer period. After being turned off, the system vibration is returned to its

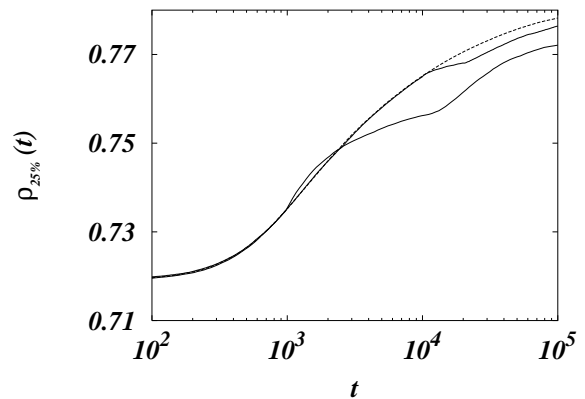


FIG. 12: Short-term memory experiment performed with the gravity driven KA model. The thick line shows the unperturbed evolution. The system is perturbed at $t_w = 10^3$ and 10^4 after evolving with $x = 0.6$ (solid normal lines). In the interval $t_w < t < t_w + \Delta t$, with $\Delta t = 10^4$, the vibration changes to 0.3. Notice that in the case where the system is perturbed earlier, the system first increases its density (the short-term memory effect as described in the text), resuming its expected behavior after some time. In the case of a later perturbation, this first regime is not noticeable.

previous values. As can be seen in figure 13 the system evolves much less during the time interval Δt when it is perturbed: the h_{cm} roughly follows a plateau. This is expected since the relaxation rate decreases for smaller values of x . Moreover, when turning the perturbation off, the system returns to a point very close to the one where it was before being perturbed. This is more clear in the inset of the same figure, where the perturbed data for $t > t_w + \Delta t$ are shifted by Δt and seems, as a first approximation, to collapse on the unperturbed curve, showing that the system keeps, to some extent, memory of its state before the perturbation even if being perturbed for a long time.

As is common in systems in a non-stationary state, the response of the system to a perturbation in the vibration clearly depends on its age. The larger is t_w , the greater is the compaction achieved by the bulk and less responsive the system becomes. For small t_w , the bulk is still very sensitive to the perturbations, the amount of free volume is considerable and as soon as the vibration is lowered, the particles get closer and the density increases very fast, even faster than one would expect from the knowledge of the asymptotic behavior. By increasing, instead of decreasing, the vibration, the opposite behavior is observed. Thus, short-term memory is related to perturbations at early times. However, as t_w increases, the amount of free volume in the bulk decreases and most of the instantaneous response, when perturbed, comes from the interface, that has a fast dynamics. After this strong response due to the interface (that is only seen in global measures like the height of the center of mass), the system continues at a much smaller pace, corresponding to the

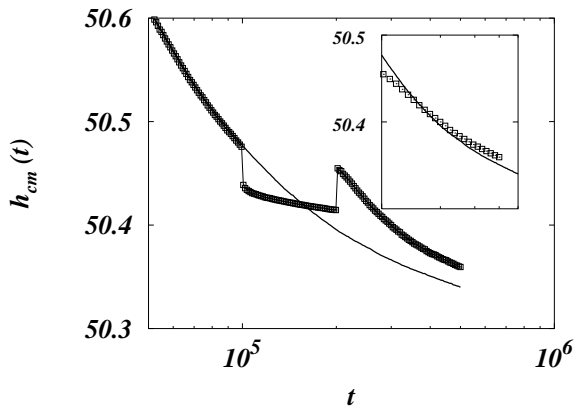


FIG. 13: Long-term memory experiment. The evolution of the height of the center of mass (or, equivalently, the potential energy) is plotted as a function of time. Notice that if the system has evolved enough time ($t_w = 10^5$ in this case) the further evolution after the perturbation is quite small and the system returns to its previous state when the perturbation is turned off. In the inset, the perturbed data for $t > t_w$ are shifted, $t \rightarrow t - 10^5$ showing that they collapse on the unperturbed data. Averages are over 300 samples.

expected evolution at the new vibration value. Thus, in the interval Δt while the perturbation is on, the amount of change is due to the bulk evolution and is smaller the larger is t_w (for example, for the waiting times that we probed, from 10^3 until 10^5 , the bulk always evolved). As a conclusion, “long-term memory” effects can only be seen as an approximation, with a very simple explanation as also pointed out in [24].

As remarked in Refs. [40] and [41] (in the context of glasses), a rate equation for a single macroscopic variable (e.g., the free volume) would not be able to account for the complexities of the memory effects. Nevertheless, it must be emphasized that the nonlinear diffusion equation studied here is explicitly dependent on the spatial dimension, and is this heterogeneous profile that encodes the additional information responsible for the effects discussed here. However, more complex memory effects are observed in systems without gravity like glasses and spin-glasses, and is unlikely that this equation would be able to account for them, since probably they involve effects due to the interaction. In order to capture the complexity of these effects, this equation would have to be properly generalized.

VI. PHYSICAL AGING UNDER GRAVITY

We now turn to the discussion of physical aging phenomena under gravity as they appear in the two-time scaling behavior after a sudden quench into the high packing density phase.

A. Mean-square displacement

In our approach the aging effects are best studied by considering the two-times mean square displacement of particles, $B(t, t_w)$, which for the 3D lattice-gas is defined as

$$B(t, t_w) = \frac{1}{3N} \sum_{a=1}^3 \sum_{k=1}^N \left\langle [r_k^a(t + t_w) - r_k^a(t_w)]^2 \right\rangle, \quad (26)$$

where $r_k^a(t)$ are the coordinates ($a = 1, 2, 3$) of the particles k at times t . In the continuous 1D diffusion model, if t is sufficiently larger than t_w , the mean-square displacement at height z can be written as

$$B_z(t, t_w) = \int_{t_w}^t ds \Gamma[\rho(z, s)]. \quad (27)$$

It is worth to recall that in zero gravity one finds a simple aging [36]. For a power-law diffusion and for the lower layers $z < z_0(\rho_R)$ we find, to leading order in t and t_w , a two-time scaling of the form

$$B_z(t, t_w) \sim t_w^{1-\mu} - t^{1-\mu}, \quad (28)$$

with an exponent $\mu = \phi/(\phi - 1)$. Since, usually $\phi > 1$, this corresponds to a super-aging regime, $\mu > 1$. This means that the effective structural relaxation time grows as t_w^μ , what is faster than the age of the system, t_w . It also means that there is a microscopic time scale that starts to become relevant, differently from what happens with simple aging. For the upper layers, $z > z_0(\rho_R)$ one obtains the same two-time scaling behavior but this time the exponent is $\mu = \phi^2/(\phi - 1)$. However, for closed systems at not so large vibrations, the contribution from the layers above z_0 is small since most of the particles are at $z < z_0$.

A similar super-aging behavior has been observed in the simulation of the gravity-driven KA model [42] where the agreement is rather good if the vibration is not too low. For example, we show in fig. 14 the mean square displacement for the case $x = 0.4$ along with fig. 15 where these curves were collapsed onto a master curve following the above scaling. The super-aging exponent obtained from the data collapse is $\mu = 1.48$ which is in very good agreement with the theoretical prediction $\mu = \phi/(\phi - 1) \simeq 1.476$. For smaller vibrations, the exponents become smaller since the time accessible to the measurement is probably not enough to reach the asymptotic regime (where the approximation is valid), thus differing from the theoretical value.

For a Vogel-Fulcher diffusion instead we find, to the leading order in t and t_w , and for $z < z_0(\rho_R)$:

$$B_z(t, t_w) \sim \log\left(\frac{t}{t_w}\right), \quad (29)$$

that is a simple aging scenario, whereas for the upper layers, $z > z_0(\rho_R)$, one obtains (to the leading order in

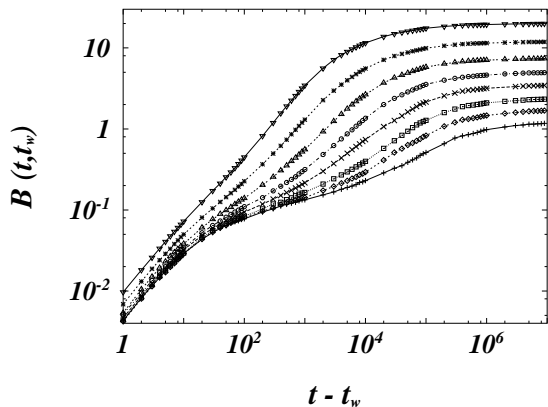


FIG. 14: Mean squared displacement $B(t, t_w)$ for waiting times $t_w = 2^{10+k}$ ($k = 1, 2, \dots$) and vibration amplitude $x = 0.4$.

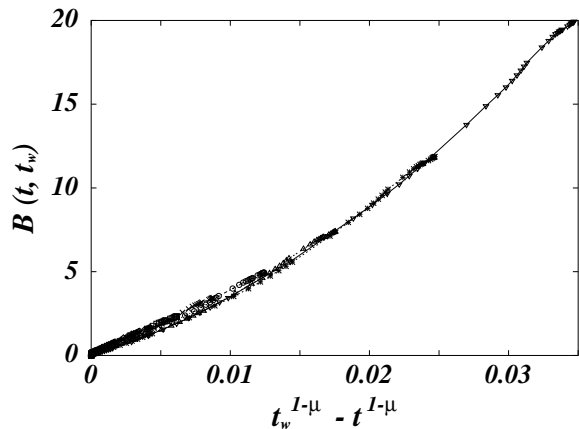


FIG. 15: Mean squared displacement $B(t, t_w)$ for several values of t_w and $x = 0.4$ as a function of $t_w^{1-\mu} - t^{1-\mu}$. The data collapse is obtained for $\mu = 1.48$.

t and t_w) that the two-time scaling does not depend on t/t_w but rather

$$B_z(t, t_w) \sim e^{-\rho c t_w} - e^{-\rho c t}. \quad (30)$$

B. Triangle relation

It is interesting to observe the different behavior of Eqs. 29 and 28 at finite waiting times t_w . In the case of simple aging, $\lim_{t \rightarrow \infty} B(t, t_w) = \infty$, i.e., a weak ergodicity scenario [43]; while for super-aging, a finite limit is obtained (which, however, vanishes as $t_w \rightarrow \infty$). The manner in which time-translation invariance is violated is, however, similar. Indeed, if we consider the “triangle relation”, $B(t_1, t_3) = f[B(t_1, t_2), B(t_2, t_3)]$, where the times t_1, t_2 , and t_3 are in increasing order, it is straightforward to check that $f(x, y) = x + y$ in both Vogel-Fulcher and power law cases, implying that displacements

over non-overlapping time intervals are statistically independent. This feature does not hold in the presence of activated aging for which $B(t, t_w) \sim \log t / \log t_w$ [43]. In the gravity driven KA model the triangle relation is not obeyed at short times but becomes asymptotically valid at longer times as it can be seen in fig. 16, [51].

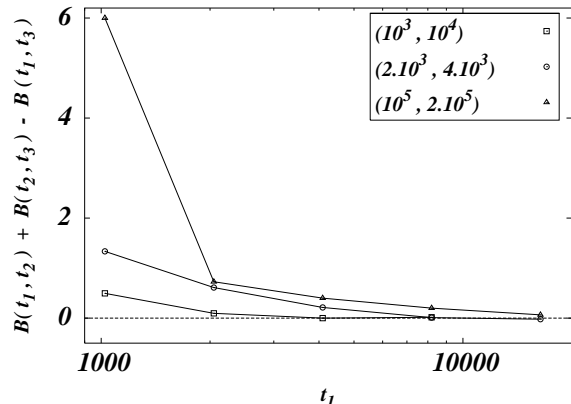


FIG. 16: Check of the triangle relation for the mean squared displacement $B(t, t')$ for $x = 0.1$. Different symbols stand for different pairs (t_2, t_3) as indicated in the figure.

VII. DYNAMIC HETEROGENEITIES

In purely kinetic models, the absence of an increasing static correlation length on approaching the dynamic arrest poses the question of whether the increasing relaxation times can be related to a diverging dynamic correlation length. This has been associated to the presence of dynamical heterogeneities in glasses (for a review see [25, 26, 32] and references therein). If the glass/dense granular analogy holds true then one would expect that the role played by dynamical heterogeneities in slow granular compaction should be similar to that observed in glassy dynamics. However, the role played by these structures and the associated lengths, on the dynamics of granular and colloidal systems, is yet to be understood. Several measures for quantifying the spatial heterogeneities have been introduced for kinetic models [32]. In particular, this issue was recently investigated in the KA model [44] without gravity using a fourth-order correlation function. Here we study the role played by these structures in the non-zero gravity case.

In figure 17 we plot the dynamical nonlinear response

$$\chi_4(z, t) = N \left(\langle q^2(z, t) \rangle - \langle q(z, t) \rangle^2 \right) \quad (31)$$

where N is the number of involved sites in the computation, $q(z, t) = C(z, t)/C(z, 0)$ and

$$C(z, t) = \frac{1}{N} \sum_i n_i(t) n_i(0) - \rho(z, t) \rho(z, 0) \quad (32)$$

where i runs over all sites in the z , $z-1$ and $z+1$ layers. Consistently with the theoretical expectation [32], the long time limit of χ_4 converges to unit, $\chi_4(z, \infty) = 1$ [52]. We also verified that this asymptotic behavior is valid in absence of gravity at variance with the results of Ref. [44] [53]. Analogously to what happens in the KA model without gravity and in other glassy systems, the peak is shifted to higher times and gets larger as the density increases (the lower is z , the greater is the density). In the inset of fig. 17 we show that both the position and height of the peak grow as power laws as the density of the corresponding height approaches ρ_c . Interestingly, χ_4 only depends on the local density: for example, in fig. 17 is shown that two curves corresponding to different z and x , but having almost the same density, are coincident within the numerical accuracy.

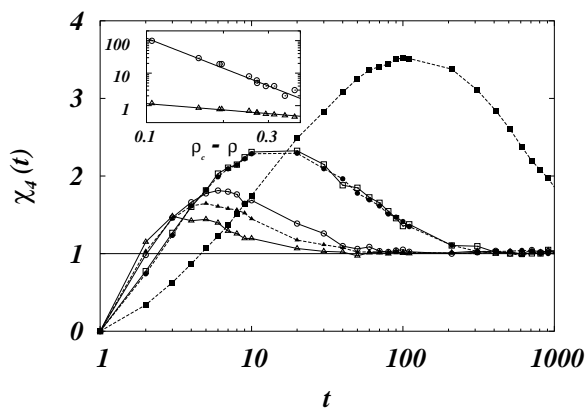


FIG. 17: Dynamical response, eq. 31, as a function of time (in MCS) for different vibrations: $x=0.92$ (filled symbols) and 0.94 (empty symbols). Different symbols stand for different heights: $z = 5, 10$ and 15 (square, circle, triangle, respectively). The line is the asymptotic $\chi_4 = 1$ behavior. Notice in the figure the presence of two very close curves: they correspond to different vibrations and heights, but their density is the same within the numerical accuracy. Inset: location (circles) and height (triangles) of the maximum of χ_4 . Both diverge as power laws with approximate exponents 3 and 0.6, respectively.

VIII. CONCLUSIONS

We have investigated some aspects of slow granular dynamics inspired by kinetic lattice-gas models [15, 31]. The key ingredient of these models is a free-volume restriction implemented by a purely kinetic constraint. No interaction between the particles is assumed beyond the hard core exclusion. The thermodynamics of the model is completely trivial and all its interesting features are purely dynamical. A macroscopic transport equation was written and studied, allowing us to predict the specific location of a jamming transition and to analyze the behavior of the system in its vicinity.

As noted in the earlier work [20] and detailed here, the time evolution of particle density in a gravity driven lattice gas is completely controlled by the mobility of the corresponding gravitationless system. It was shown that for a power law mobility, the bulk density relaxes as a power law. On the other hand, when the particle diffusion decreases exponentially accordingly to the Vogel-Fulcher law, a logarithmically slow compaction is found. Due to the finite time window available, the data on granular systems from the Monte Carlo simulation, as well as from experiments, is consistent with both the power law and logarithmic relaxation. Furthermore, the issue of whether the asymptotic density is a monotonic function of the vibration amplitude, can only be solved by performing simulations over a much larger time window [37]. For the maximum time achieved here, the asymptotic packing density seems to depend on the vibration strength in a non trivial way.

The similarities between granular and glassy systems have been stressed many times in recent years. Here we extended this discussion by showing that the behavior of dynamical heterogeneities is quite similar to the ones present in systems without gravity. We showed that for different vibrations the global non homogeneity induced by gravity (that is, the density profile, different for each vibration) does not affect the local character of these quantities that only depends on the local density: the heterogeneities present in a horizontal layer depends only on this layer density. This result could also be relevant to the investigation of slow sedimentation of colloids.

Other signatures of glassy behavior are also present, like aging, reversible-irreversible cycles and memory effects. In particular, short and long-term memory effects are simpler than their glassy counterpart and have already been described in terms of the density profile properties. Irreversible branches are obtained when cycling the vibration amplitude, approaching a quasi-reversible branch when the rate is slow enough or after cycling many times. We also remark the analogy between short-term memory effects and the cycling experiments. In the decreasing- x part of the cycles, the density increases as for smaller x . This is at variance with what one would expect from the long time behavior of the asymptotic packing density, exactly in the same way as the system behaves in short-term memory experiments. The difference is that in one case the change in vibration is discontinuous while in the other, it is done at a small rate.

The analytical approach presented here has some limitations. Among the features seen in the simulation, which are not properly described by the theory, are: existence of a dense layer between the bulk and the interface and the initial state dependent oscillations at the bottom of the sample. These may be a direct consequence of the local density approximation used for the mobility. A weighted density approximation might be able to account for some of these features. Moreover, since the equation is deterministic, fluctuation dependent quantities (e.g., $\chi_4(t)$) are not captured by the formalism and

noise has to be included [45].

Another interesting question concerns the role of friction. In realistic systems, the energy injected by stirring, shearing, tapping etc. is dissipated by the inelastic collisions among the particles, creating a gradient of granular temperature [46, 47, 48]. Here we assume that the system is in contact with a thermal bath, a situation which is quite different. In highly packed granular systems however the steric hindrance is far more important than the energy dissipation, as one is able to reproduce several features of compaction dynamics by ignoring the specific mechanism of energy injection/dissipation.

Finally, we mention that slow relaxation in the KA model has also been analyzed in terms of the dynamically available volume, expressed by holes density ν [49]. A hole is defined as an empty site where a neighbouring particle satisfies the kinetic constraints and may jump in. It has been recently suggested that dynamical arrest in different systems, such as glasses, colloids, gels, compressed emulsion and granulars, has a universal character when described in terms of ν . In particular, as one approaches the transition, the diffusion coefficient goes to zero as a

power-law $D = (\nu - \nu_0)^\gamma$, where ν_0 is the residual density of rattlers that do not contribute to the macroscopic diffusion, and γ is an universal exponent that assume the value $\gamma = 2$ irrespective of the system considered [49]. It would be interesting to investigate to what extent the presence of gravity, and consequently of a heterogeneous density profile might modify the above results.

In conclusion, nonlinear diffusion equation and kinetically constrained models, in spite of their simplicity, seem to capture the main dynamical features of dense granular materials and provide a natural framework in which slow relaxation phenomena in granular and glassy matter can be easily understood.

Acknowledgments

This work was supported in part by the Brazilian agencies CNPq and FAPERGS. JJA thanks the Abdus Salam ICTP for hospitality where part of this work was done.

-
- [1] S. F. Edwards, in *Granular Matter: An Interdisciplinary Approach*, edited by A. Mehta (Springer-Verlag, New York, 1994).
 - [2] P.-G. de Gennes, *Physica A* **261**, 267 (1998).
 - [3] L. P. Kadanoff, *Rev Mod. Phys.* **71**, 435 (1999).
 - [4] J. Duran, *Sands, Powders, and Grains* (Springer-Verlag, New York, 2000).
 - [5] L. C. E. Struik, *Physical Aging in Amorphous Polymers and Other Materials* (Elsevier, Amsterdam, 1978).
 - [6] S. F. Edwards, in *Disorder in Condensed Matter Physics*, edited by J. A. Blackman and J. Tagüeña (Clarendon, Oxford, 1991).
 - [7] J. B. Knight, C. G. Fandrich, C. N. Lau, H. M. Jaeger, and S. R. Nagel, *Phys. Rev. E* **51**, 3957 (1995).
 - [8] E. R. Nowak, J. B. Knight, M. L. Povinelli, H. M. Jaeger, and S. R. Nagel, *Powder Technology* **94**, 79 (1997).
 - [9] E. R. Nowak, J. B. Knight, E. Ben-Naim, H. M. Jaeger, and S. R. Nagel, *Phys. Rev. E* **57**, 1971 (1998).
 - [10] F. X. Villarruel, B. E. Lauderdale, D. M. Mueth, and H. M. Jaeger, *Phys. Rev. E* **61**, 6914 (2000).
 - [11] G. D'Anna and G. Gremaud, *Nature* **413**, 407 (2001).
 - [12] S. Warr and J.-P. Hansen, *Europhys. Lett.* **36**, 589 (1996).
 - [13] M. Nicodemi, A. Coniglio, and H. J. Herrmann, *Phys. Rev. E* **55**, 3962 (1997).
 - [14] J. J. Brey, A. Prados, and B. Sánchez-Rey, *Phys. Rev. E* **60**, 5685 (1999).
 - [15] M. Sellitto and J. J. Arenzon, *Phys. Rev. E* **62**, 7793 (2000).
 - [16] A. Barrat and V. Loreto, *J. Phys. A* **33**, 4401 (2000).
 - [17] P. Philippe and D. Bideau, *Phys. Rev. E* **63**, 051304 (2001).
 - [18] J. Berg and A. Mehta, *Europhys. Lett.* **56**, 784 (2001).
 - [19] C. Fusco, A. Fasolino, P. Gallo, A. Petri, and M. Rovere, *Phys. Rev. E* **66**, 031301 (2002).
 - [20] Y. Levin, J. J. Arenzon, and M. Sellitto, *Europhys. Lett.* **55**, 767 (2001).
 - [21] C. Jossierand, A. V. Tkachenko, D. M. Mueth, and H. M. Jaeger, *Phys. Rev. Lett.* **85**, 3632 (2000).
 - [22] M. Nicolas, P. Duru, and O. Pouliquen, *Eur. Phys. J. E* **3**, 309 (2000).
 - [23] J. J. Brey and A. Prados, *Phys. Rev. E* **63**, 061301 (2001).
 - [24] A. Barrat and V. Loreto, *Europhys. Lett.* **53**, 297 (2001).
 - [25] H. Sillescu, *J. of Non-Cryst. Sol.* **243**, 81 (1999).
 - [26] R. Richert, *J. Phys.: Condens. Matter* **14**, R703 (2002).
 - [27] Y. Levin, *Physica A* **287**, 100 (2000).
 - [28] W. Götze and L. Sjögren, *Rep. Prog. Phys.* **55**, 241 (1992).
 - [29] M. Tokuyama and I. Oppenheim, *Physica A* **216**, 85 (1995).
 - [30] W. van Meegen, T. C. Mortensen, S. R. Williams, and J. Müller, *Phys. Rev. E* **58**, 6073 (1998).
 - [31] W. Kob and H. C. Andersen, *Phys. Rev. E* **48**, 4364 (1993).
 - [32] F. Ritort and P. Sollich, cond-mat/0210382 (unpublished).
 - [33] A. Imparato and L. Peliti, *Phys. Lett. A* **269**, 154 (2000).
 - [34] E. Clement and J. Rajchenbach, *Europhys. Lett.* **16**, 133 (1991).
 - [35] O. Pouliquen, M. Nicolas, and P. D. Weidman, *Phys. Rev. Lett.* **79**, 3640 (1997).
 - [36] L. Peliti and M. Sellitto, *J. Phys. IV France* **8**, Pr6 (1998).
 - [37] D. A. Head, *Phys. Rev. E* **62**, 2439 (2000).
 - [38] T. Boutreux and P.-G. de Gennes, *Physica A* **244**, 59 (1997).
 - [39] J. J. Brey, A. Prados, and B. Sánchez-Reys, *Physica A* **284**, 277 (2000).
 - [40] J. P. Bouchaud, cond-mat/0211196 (unpublished).
 - [41] A. J. Kovacs, *Adv. Polym. Sci.* **3**, 394 (1963).

- [42] M. Sellitto, Phys. Rev. E **63**, 060301(R) (2001).
- [43] J.-P. Bouchaud, L. Cugliandolo, J. Kurchan, and M. Mézard, in *Spin-glasses and random fields*, edited by A.P. Young (World Scientific, Singapore, 1997).
- [44] S. Franz, R. Mulet, and G. Parisi, Phys. Rev. E **65**, 021506 (2002).
- [45] D. A. Stariolo, Phys. Rev. E **55**, 4806 (1997).
- [46] R. D. Wildman, J. M. Huntley, J.-P. Hansen, D. J. Parker, and D. A. Allen, Phys. Rev. E **62**, 3826 (2000).
- [47] R. D. Wildman, J. M. Huntley, and D. J. Parker, Phys. Rev. E **63**, 061311 (2001).
- [48] X. Yang, C. Huan, D. Candela, R. W. Mair, and R. L. Walsworth, Phys. Rev. Lett. **88**, 044301 (2002).
- [49] A. Lawlor, D. Reagan, G. D. McCullagh, P. de Gregorio, P. Tartaglia, and K. A. Dawson, Phys. Rev. Lett. **89**, 245503 (2002).
- [50] The effect of dissipation can be studied by allowing for violation of detailed balance, as recently done for example in Ref. [19].
- [51] We thank J. Kurchan for suggesting to check the triangle relation.
- [52] We thank P. Sollich for discussions on this point
- [53] We thank R. Mulet for discussions on this point